



Tuning the ultrasonic and photoacoustic response of polydopamine-stabilized perfluorocarbon contrast agents

Journal:	<i>Journal of Materials Chemistry B</i>
Manuscript ID	TB-ART-05-2019-000928.R1
Article Type:	Paper
Date Submitted by the Author:	25-Jun-2019
Complete List of Authors:	Xie, Yijun; University of California San Diego Wang, Junxin; University of California San Diego, Department of NanoEngineering Wang, James; University of California San Diego Hu, Ziyang; Northwestern University Hariri, Ali; University of California San Diego Department of Nanoengineering, Tu, Nicholas; University of California San Diego Krug, Kelsey; University of California San Diego Burkart, Michael; University of California San Diego Gianneschi, Nathan; Northwestern University; University of California San Diego Jokerst, Jesse; University of California San Diego, Rinehart, Jeffrey; University of California San Diego

ARTICLE

Tuning the ultrasonic and photoacoustic response of polydopamine-stabilized perfluorocarbon contrast agents

Received 00th January 20xx,
Accepted 00th January 20xx

Yijun Xie^{‡,a,b}, Junxin Wang^{‡,c}, James Wang^c, Ziyang Hu^d, Ali Hariri^c, Nicholas Tu^a, Kelsey A. Krug^a, Michael D. Burkart^a, Nathan C. Gianneschi^d, Jesse V. Jokerst^{*,c}, and Jeffrey D. Rinehart^{*,a,b}

DOI: 10.1039/x0xx00000x

Contrast-enhanced ultrasound (CEUS) offers the exciting prospect of retaining the ease of ultrasound imaging while enhancing imaging clarity, diagnostic specificity, and theranostic capability. To advance the capabilities of CEUS, the synthesis and understanding of new ultrasound contrast agents (UCAs) is a necessity. Many UCAs are nano- or micro-scale materials composed of a perfluorocarbon (PFC) and stabilizer that synergistically induce an ultrasound response that is both information-rich and easily differentiated from natural tissue. In this work, we probe the extent to which CEUS is modulated through variation in a PFC stabilized with fluorine-modified polydopamine nanoparticles (PDA NPs). The high level of synthetic tunability in this system allows us to study signal as a function of particle aggregation and PFC volatility in a systematic manner. Separation of aggregated and non-aggregated nanoparticles lead to a fundamentally different signal response, and for this system, PFC volatility has little effect on CEUS intensity despite a range of over 50°C in boiling point. To further explore the imaging tunability and multimodality, Fe³⁺-chelation was employed to generate an enhanced photoacoustic (PA) signal in addition to the US signal. *In vitro* and *In vivo* results demonstrate that PFC-loaded PDA NPs show stronger PA signal than the non-PFC ones, indicating that the PA signal can be used for in situ differentiation between PFC-loading levels. In sum, these data evince the rich role synthetic chemistry can play in guiding new directions of development for UCAs.

Introduction

In many ways, ultrasonography is an ideal medical imaging technique – equipment and maintenance costs are comparatively minor, safety concerns are minimal, portability is high, and time resolution can exceed high-frame-rate cinema by orders of magnitude. As a complement to more intensive techniques such as magnetic resonance imaging (MRI), positron emission tomography (PET) and computed tomography (CT), US has become ubiquitous in diagnostic imaging.^{1–4} By introducing an ultrasound contrast agent (UCA), utility can be further enhanced, allowing better tracking of blood flow rates, sharpening of contrast in tissue density, and enhanced resolution.^{5, 6} Although there are many ways in which an ultrasound wave can interact with a contrast agent to generate a detectable signal, they involve classical wave mechanics describing the motion, density, and elasticity of the agent relative to the medium. Thus, a balance must be struck between

tissue penetration, signal resolution, and contrast with surrounding tissue. Strong contrast signals at common ultrasound transducer frequencies can be obtained with inert gases or encased volatile liquid droplets due to their low densities relative to biological tissue. Many commercial ultrasound agents employ perfluorocarbons (PFC) stabilized by protein, polymer or lipid shells, as these are biocompatible and their compressibility and low boiling point enhances the interaction with ultrasound energy.^{7–9} While ideal for many applications, US contrast agents of this type have several limiting factors. One challenge is fine-tuning the strength of PFC encapsulation. Weaker encapsulation leads to strong bursts of contrast with minimal ultrasound power, but it also limits the useful imaging time window due to the volatility of PFC. Another challenge is the synthetic complexity required for tuning the ultrasonic response, altering the size, or introducing new functionality.

Previously we demonstrated a system where instead of encapsulation within a core-shell structure, PFC could be stabilized in aqueous suspension by association with non-porous polydopamine nanoparticles (PDA NPs) functionalized with a perfluorinated alkane.¹⁰ This system shows a surprisingly strong and long-lived contrast response with reasonable colloidal stability, which may arise from the balance of fluororous components (PDA NPs and PFC) and polar components (PDA NPs and H₂O).^{11, 12} This long-lived, strong signal and highly tunable synthetic platform offers an intriguing system to explore both the fundamental nature of the acoustic response and the extent to which its properties can be enhanced for

^a Department of Chemistry and Biochemistry, University of California, San Diego, La Jolla, CA 92093, USA.

^b Materials Science and Engineering Program, University of California, San Diego, La Jolla, CA 92093, USA.

^c Department of NanoEngineering, University of California, San Diego, La Jolla, CA 92093, USA.

^d Department of Chemistry, Northwestern University, Evanston, IL 60208, USA.

[‡] Authors contributed equally to the work.

Electronic Supplementary Information (ESI) available: SEM and TEM images for other PDA particles, DLS data, EDS spectra, UV-vis spectra, other color Doppler and CPS images for the control sample and PDAF-% samples and quantitative results, *ex vivo* US and PA imaging for tissues. See DOI: 10.1039/x0xx00000x

potential implementation in CEUS. To advance these aims, we have improved upon our initial synthetic methods to prepare 1H,1H,2H,2H-perfluorodecanethiol-functionalized PDA with better aqueous colloidal stability and greater control over aggregation. Importantly, our new synthetic methods allow study of how aggregation of PDA/PFC within aqueous suspension affects the ultrasound response. Results show that there is a fundamentally different power response between the isolated particles and Pickering microscale emulsion aggregates in the colloidal suspension of our material.¹³⁻¹⁵ Additionally, this work explores the ways in which imaging contrast, stability, and multimodality are controlled and enhanced including introduction of chelating metals, decreased PFC volatility, and long timescale storage and measurement of materials. We probe the system's durability under *ex vivo*, *in vitro* cell viability, and *in vivo* conditions and its multimodality with photoacoustic (PA) contrast—a hybrid technique that combines optical contrast and acoustic spatial/temporal resolution.^{16, 17} The combination of PDA-based imaging by CEUS and PA adds additional modalities to complement and track the myriad biomedical applications currently under exploration for PDA and other synthetic melanin particles.¹⁸⁻²⁴

Experimental Section

Materials

Dopamine hydrochloride (DA, 99%) and perfluorohexanes (PFH) was purchased from Alfa Aesar. Ammonium hydroxide ($\text{NH}_3 \cdot \text{H}_2\text{O}$, 28%-30%) was purchased from VWR International. 1H,1H,2H,2H-Perfluorodecanethiol (97%) was purchased from Sigma-Aldrich. Perfluoropentane (PFP) was purchased from Strem Chemicals. Iron(III) chloride hexahydrate ($\text{FeCl}_3 \cdot 6\text{H}_2\text{O}$, 98%) and ethanol (100%) was obtained from Fisher Scientific. Perfluorobutane (PFB) was purchased from SynQuest Labs. All chemicals were used without further purifications. Deionized water is used in all the experiments.

Synthesis of PDA-Fe-*i*% NPs

PDA-Fe-0.13% NPs were synthesized using ethanol-water system by modifying the reported methods.^{10, 25-27} Briefly, 60 mg of DA was mixed with 20 mL of ethanol and 60 mL of water under stirring, and subsequently 8 mg of $\text{FeCl}_3 \cdot 6\text{H}_2\text{O}$ in 20 mL of water was added to the mixture. After vigorous stirring for 10 min, 20 mL of water containing 500 μL of $\text{NH}_3 \cdot \text{H}_2\text{O}$ was quickly added to the mixed solution. After stirring for 24 h at room temperature, the product is centrifuged and washed with deionized water three times. In the case of PDA-Fe-1.0%, PDA-Fe-1.7%, and PDA-Fe-2.4% NPs, the amount of $\text{FeCl}_3 \cdot 6\text{H}_2\text{O}$ and $\text{NH}_3 \cdot \text{H}_2\text{O}$ used is 12 mg and 600 μL for PDA-Fe-1.0%, 16 mg and 980 μL for PDA-Fe-1.7%, 20 mg and 1000 μL for PDA-Fe-2.4% NPs, respectively.

Synthesis of PDAF-*i*% NPs

PDAF-0.13% NPs were synthesized by functionalizing PDA-Fe-0.13% with 1H,1H,2H,2H-perfluorodecanethiol. First, the PDAF-0.13% particles obtained from the previous step was mixed with 10 mL of ethanol and 40 mL of water. Then 60 μL of 1H,1H,2H,2H-Perfluorodecanethiol was added to the mixed solution. After 5 min of vigorous stirring, 10 mL of water containing 150 μL of $\text{NH}_3 \cdot \text{H}_2\text{O}$ was quickly added to the mixture. After stirring for 24 h, the particles are separated by centrifugation and washed with water and ethanol three times, and the final product is PDAF-0.13%. PDAF-1.0%, PDAF-1.7%, and PDAF-2.4% are prepared in the same method using PDA-Fe-1.0%, PDA-Fe-1.7%, PDA-Fe-2.4%, respectively.

Preparation of PFC-loaded PDAF-*i*% NPs

PFC-loaded PDAF-*i*% NPs were prepared with the typical immersion method.^{10, 28} PDAF-*i*% particles are first lyophilized at -55°C under 0.04 mbar overnight. Then 1 mg of PDAF-*i*% particles were dispersed in 200 μL of PFC and sonicated for 10 s (Fisher Scientific MH ultrasonic bath, 70 W, 40 kHz), evaporating the excess PFC until no PFC liquid was seen in the vial. After that, 2 mL of deionized water was added to the mixture and sonicated for another 10 s. The mixed solution was used for imaging experiments. Low speed centrifugation was performed by centrifuging the mixed solution at 2500 rpm for 3 min; the supernatant (PDAF-small) and precipitate (PDAF-large) were collected for the imaging experiments.

Characterizations

TEM images were acquired on an FEI Tecnai G2 Spirit TEM operating at 120 kV. SEM images and elemental analysis were obtained by an FEI Quanta 250 SEM equipped with a Thermo Fisher Scientific EDS detector. STEM images and EDS spectra maps were acquired using a Hitachi HD-2300 Dual EDS Cryo STEM equipped with dual Thermo Fisher Scientific EDS detectors. The Hitachi HD-2300 was operated at 200 kV. DLS and zeta potential measurements were determined by Malvern Zetasizer Nano ZS90. XPS analysis was conducted on Thermo Fisher Scientific ESCALab 250Xi spectrometer using Al K-alpha X-ray source (1486.6 eV). The XPS spectra were calibrated with adventitious carbon peak at 284.8 eV. UV-vis spectra were measured on a PerkinElmer Lambda 35 UV/vis spectrophotometer. Optical microscope images were taken on an EVOS FL Auto Imaging System under transmitted light imaging mode.

Ultrasound imaging

Ultrasound imaging was collected on a Siemens Sequoia 512 with an Acuson 15L8 transducer at 7 MHz. 0.5 mg mL^{-1} of PDA particles in aqueous dispersions was tested for *in vitro* ultrasound imaging. Both color Doppler and CPS imaging were used for ultrasound imaging experiments. Both color Doppler and CPS modes are performed with the increase of MI from 0.06 to 1.9. CPS imaging was used at 7 MHz and image brightness was quantified by averaging the brightness over the region of

interest using MATLAB R2016b. Continuous imaging was performed by imaging at color Doppler mode at MI=1.9 until the signal decayed to the intensity of deionized water signal.

Ex vivo cardiac ultrasound experiments

100 μL of PFP-loaded PDAF-2.4% with 4 mg mL^{-1} was injected into the left ventricle of a chicken heart (2.5 cm \times 3 cm). Color Doppler imaging commenced immediately after injection with an increase in MI from 0.06 to 1.9. Control experiments were performed by injecting deionized water into the tissue.

Photoacoustic imaging

Photoacoustic imaging was performed on a VisualSonics Vevo 2100 LAZR imaging system. Transducers with the frequency of 21 MHz and 40 MHz were used for the experiments. For *in vitro* experiments, 17 μL of PDA particles with 0.5 mg mL^{-1} was used for imaging at 21 MHz with pulsed laser excitation at 700 nm. ImageJ was used to quantify the PA signal. For the *ex vivo* experiments, PDAF-2.4% NPs (4 mg mL^{-1}) with 100 μL were injected into fresh chicken breast tissue (7 cm \times 8 cm). PA as well as B-mode images were collected at the frequency of 40 MHz and laser wavelength of 700 nm.

Cytotoxicity assay

HCT116 colorectal carcinoma cells were plated at 2.5×10^3 cells/well in DMEM high glucose (Corning) + 10% FBS. Cells were grown for 24 hours and then treated with PDAF-*i*% NPs (pre-solubilized in H_2O) ranging from concentrations of 0–500 $\mu\text{g}/\text{ml}$ for 24 hours. Then, the cells were washed twice with PBS, and 100 μL of media was added to each well, followed by 20 μL of CellTiter Aqueous One Solution (Promega). After 3 hours at 37 $^\circ\text{C}$, solutions were centrifuged at 10,000 RPM for 10 minutes, three times, and supernatant was transferred to a new plate. Then absorbance readings were taken at 490 nm (test wavelength) and 690 nm (reference wavelength).

In vivo ultrasound and photoacoustic imaging

All animal studies were performed in accordance with the guidelines of the Institutional Animal Care and Use Committee (IACUC) at the University of California, San Diego. All experiments followed the guidelines of the Institutional Animal Care and Use Committee at the University of California, San Diego. The protocol was approved by the Institutional Animal Care and Use Committee at the University of California, San Diego. Colloidal suspensions of PDAF-2.4% NPs (1, 2, 4, and 8 mg mL^{-1} , 50 μL) with or without PFH loading were mixed with Matrigel in a 1:1 ratio and subcutaneously injected into the loose skin over the back of a 5-month old nude mouse via an insulin syringe (BD Micro-Fine™). Due to timing and equipment constraints, prepared mixtures were transferred to the IACUC and stored at 4 $^\circ\text{C}$ for 4.5 h before *in vivo* experiments. The photoacoustic and color Doppler images were collected using the same VisualSonics LAZR photoacoustic scanner with a LZ550

transducer at 37 dB with and without 700 nm excitation, respectively. We repeated the experiment using a mixture of 50 μL Millipore water with 50 μL Matrigel as the negative control. For the signal stability measurement, the injected area was exposed to 700 nm laser for 10, 20, and 30 minutes and imaged using the photoacoustic or color Doppler mode. The photoacoustic images were exported as TIFF files and analyzed via ImageJ 1.49v.²⁹ The photoacoustic images were converted to grey scale (8 bit) and the raw integrated intensity of 6 regions of interest within one sample were measured. The limit of detection was calculated at 3 standard deviation above the average of the baseline. The color Doppler signal detection limit was estimated by comparing the signal of 2.0, 1.0, 0.5, and 0 mg/mL PDAF-PFH NPs that were subcutaneously injected in the nude mouse.

Results and discussion

PDA NPs with chelated Fe(III) ions were synthesized by a modification of a previously reported method (Figure 1a).²⁶ Briefly, FeCl_3 and 2-(3,4-dihydroxyphenyl)ethylamine (dopamine) were dissolved in a 1:5 ethanol: H_2O solution and allowed to oxidatively polymerize under basic conditions (initial pH around 10.2) for 24 h.

Isolated PDA-Fe NPs were made fluorophilic through post-synthetic attachment of 1H,1H,2H,2H-Perfluorodecanethiol via thiol Michael addition (PDAF-*i*%, *i* represents the weight percent of Fe^{3+} , *i* = 0.13, 1.0, 1.7, 2.4). Size and morphology of the modified particles were determined by transmission electron microscope (TEM) and scanning electron microscope (SEM) (Figure 1b-f, S1). With increasing initial Fe^{3+} concentration, the final NP sizes were found to show some increase in the final size (PDAF-0.13%, $d = 85 \pm 6$ nm; PDAF-1.0%, $d = 103 \pm 12$ nm; PDAF-1.7%, $d = 95 \pm 13$ nm; PDAF-2.4%, $d = 137 \pm 15$ nm). Weight percentages of the Fe^{3+} cation concentration were determined by inductively coupled plasma mass spectrometry (ICP-MS). Further decreasing the initial Fe^{3+} ion concentration does not lower the amount incorporated, nor does it decrease the NP size (Figure S2). As discussed in previous studies,¹⁸ when present during the polymerization, Fe^{3+} cation distribution in PDA is roughly homogeneous. Scanning transmission electron microscopy with energy-dispersive X-ray spectroscopy (STEM-EDS) confirm that this is also true for our NPs (Figure 1g, 1h).

SEM images (Figure 1f and S1) confirm the spherical morphology and lack of significant cross-linking of particles as observed in our previous results.¹⁰ In fact, no significant morphological or size alterations were observed after 1H,1H,2H,2H-perfluorodecanethiol functionalization, indicating that these steps are independently modifiable without the need for re-optimization of the overall experimental parameters (Figure S3). As the imaging properties of UCAs strongly depend on the particle aggregation state, dynamic light scattering (DLS) measurements were used to compare the hydrodynamic and physical sizes measured by TEM analysis. The hydrodynamic radii displayed by PDAF-*i*% display expected diameter increases that are still consistent with minimal aggregation and low polydispersity (PDAF-0.13%, $d_{\text{H}} = 167 \pm 57$ nm, PDI = 0.117; PDAF-

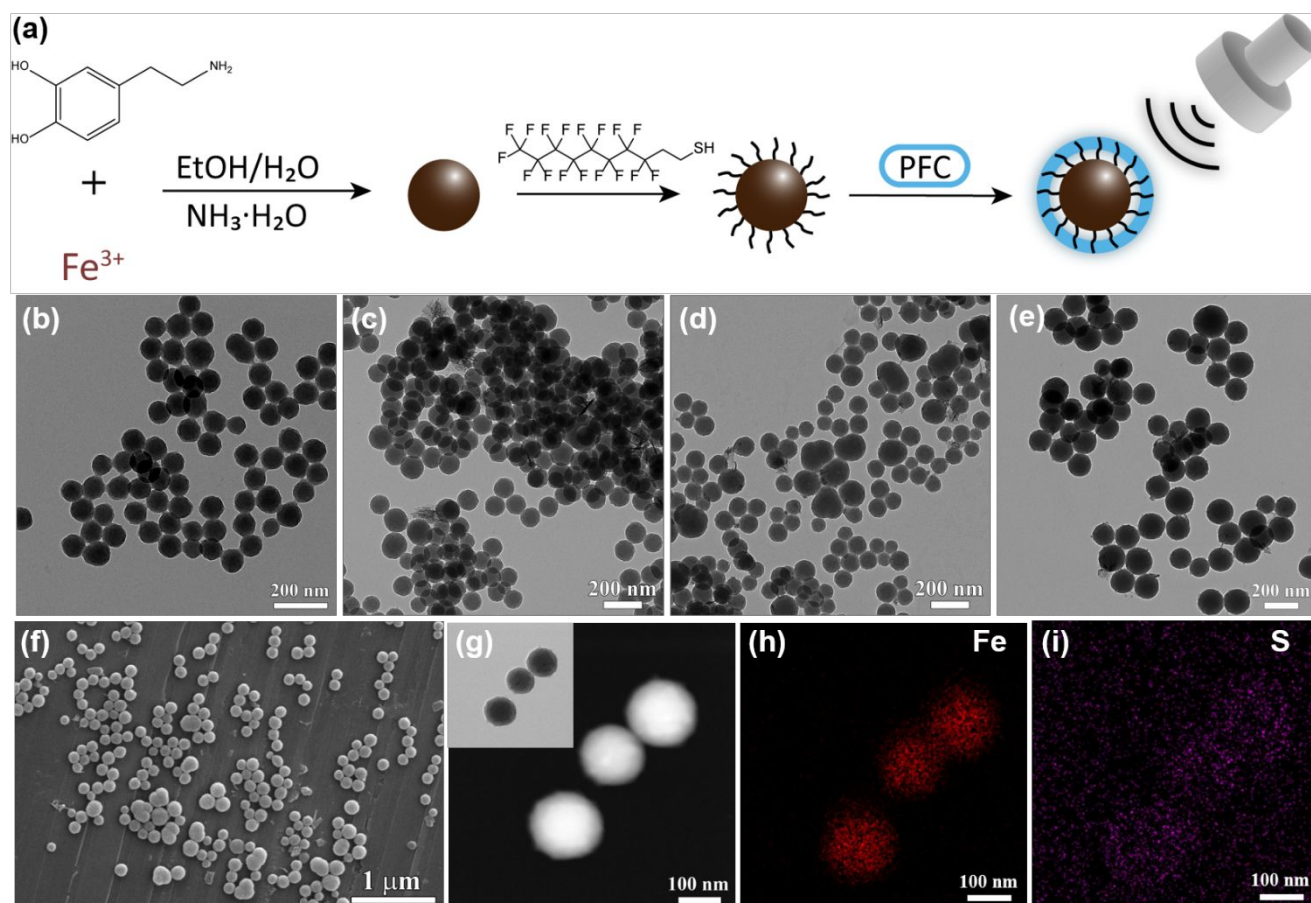


Fig. 1 (a) Schematic illustration of the synthetic procedure of PDAF-*i*% NPs. TEM images of (b) PDAF-0.13% NPs, (c) PDAF-1.0% NPs, (d) PDAF-1.7% NPs, (e) PDAF-2.4% NPs, (f) SEM image of PDAF-2.4%, (g) HAADF-STEM image of PDAF-2.4% NPs with an inset of TEM image of (e), and elemental mapping of (h) Fe, (i) S elements on PDAF-2.4% NPs.

1.0%, $d_H = 196 \pm 53$ nm, PDI = 0.074; PDAF-1.7%, $d_H = 214 \pm 55$ nm, PDI = 0.067; PDAF-2.4%, $d_H = 202 \pm 57$ nm, PDI = 0.081, Figure S4). Zeta potentials of PDAF-0.13%, PDAF-1.0%, PDAF-1.7%, and PDAF-2.4% were -32.2 ± 0.2 , -30.4 ± 1.9 , -35.3 ± 0.2 , -31.6 ± 0.4 mV, respectively, indicating good stability in aqueous solution. After PFP loading, DLS data show a detectable level of aggregation in PDAF-1.0% (PDI = 0.204) and PDAF-2.4% (PDI = 0.284), which is postulated to arise from condensation of "Pickering" PDAF-stabilized PFP-emulsion droplets in the aqueous phase (Figure S5a-d). In addition, PFP-loaded PDAF were shown to have minimal propensity to aggregate when suspended in PBS and Fetal Bovine Serum (FBS) (Figure S5e-f).

To further confirm the successful functionalization of the surface of PDA-Fe NPs with 1H,1H,2H,2H-perfluorodecanethiol, energy-dispersive X-ray spectroscopy (EDS) was employed for elemental analysis (Figure S6). The wt. % of sulfur is similar for all NP samples (4.0% for PDAF-0.13%, 3.7% for PDAF-1.0%, 2.3% for PDAF-1.7% NPs, and 3.7% for PDAF-2.4%) and indicates a surface coverage of 0.84 ± 0.19 S/nm². STEM-EDS mapping of S element shows that S element is present uniformly on the PDAF-2.4% NPs, consistent with intact incorporation (Figure 1i). To characterize fluorine in the PDA sample, X-ray photoelectron spectroscopy (XPS) was performed. The binding energy of 688

eV was attributed to the fluorine of perfluorodecanethiol (Figure S7).³⁰

To activate PDAF-*i*% NPs for use as UCAs, they must be loaded with a US responsive volatile liquid. Perfluorocarbons (PFCs) were chosen for their proven safety, chemical inertness, and ultrasound responsivity at common medical transducer frequencies.⁸ In our previous work, 1H,1H,2H,2H-perfluorodecanethiol functionalization of PDA was shown to associate with and stabilize perfluoropentane (PFP, $T_b = 28^\circ\text{C}$) in aqueous solution, thus PFP was employed to benchmark the basic capabilities of PDAF-*i*% NPs by two important UCA modalities: color Doppler and contrast pulse sequence (CPS) imaging (Figure 2). Color Doppler is the imaging signal arising from a blue or red shift of the transducer frequency usually attributed to the Doppler effect caused by fluid motion.³¹ As it shows strong and directional contrast in the presence flow, its most common use is cardiac imaging.³² Non-flowing UCA samples can also show color Doppler signal where it appears as a high-contrast speckle pattern of random Doppler shifts.³³ Strong color Doppler signal is observed for all PDAF-*i*% samples with peak brightness at the maximum mechanical index (MI = 1.9) (Figure 2, S8a-b). Although speckle patterns are difficult to quantify, the image quality roughly scaled with the particle size, with PDAF-0.13% showing the weakest signal and PDAF-2.4%

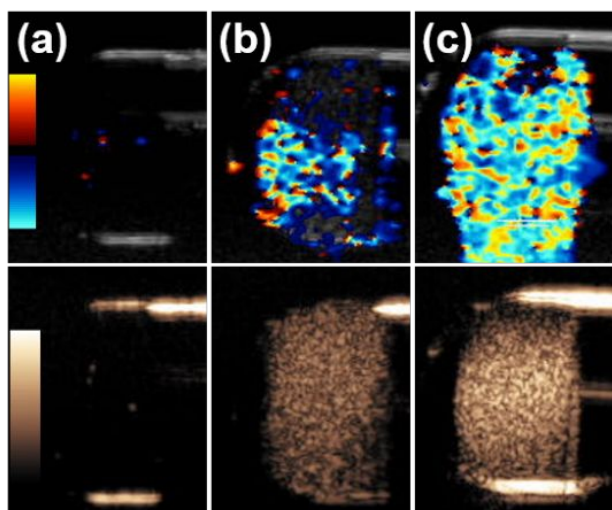


Fig. 2 Color Doppler (up) and CPS imaging (down) of PFP-loaded (a) PDA-Fe-2.4%, (b) PDAF-0.13%, (c) PDAF-2.4% (MI = 1.9; room temperature). For Color Doppler, black corresponds to no frequency shift. Warm and cool colors represent opposing frequency shifts. The grayscale signal is from simultaneously-collected B-mode imaging. For CPS images, black and white represent minimum and maximum signal intensity.

showing the strongest. This trend is logical, given that stronger acoustic cavitation and nonlinear backscattering is expected for larger particles.^{9, 34} Compared to our previous fluorinated PDA UCAs,¹⁰ PDAF-*i*% shows stronger color Doppler signal and better colloidal stability. These properties are likely due to the post-synthetic F-functionalization method which prevents interparticle crosslinking during the initial particle synthesis. PFP-loaded PDA-Fe particles without fluorine functionalization and PFP-H₂O emulsion mixtures without any particles, were also imaged using color Doppler mode. Unfunctionalized PDA NPs exhibit no color Doppler signal even at MI = 1.9, indicating that both PFP and the functionalization to induce fluorophilic stabilization are required to generate signal (Figure 2a and S8c-e). PFP-H₂O control samples also show no signal up to MI = 1.9 without stabilizing PDAF-*i*% (Figure S9a-b), demonstrating the importance of the particle in stabilizing the volatile PFP.

In addition to color Doppler, PDAF-*i*% were imaged using the Contrast Pulse Sequence (CPS) method. In this method, the non-linear ultrasound response of PFCs due to expansion and contraction is exploited to detect shifts in the phase angle. By subtraction of the linear response, virtually background-free signals can be obtained. Figure 2b-c (bottom) and S8a-b show representative CPS images for PDAF-*i*% with the golden grain pattern quantifying clear CPS response from all samples (Figure 3a-d). Quantification is performed by averaging pixel intensities such that a fully saturated signal area will result in an intensity of 255. Room temperature values for PDAF-*i*% at mechanical index (MI) = 1.9 fall in the range of 60-100 (Figure 3a-d), comparable to PFC-loaded hollow silica, and commercial UCAs,^{10, 31} All PDAF-*i*% show significant intensity at lower MI as well (MI = 1.2; Figure S9c-f).

The interaction between the PFC and PDAF is crucial to stability and the timescale of imaging. It is expected from previous results on PFH nanoemulsions,⁹ that the imaging

characteristics will be altered by changes in available thermal energy. To ensure that our UCAs are viable at body temperature, color Doppler and CPS imaging was performed at 37°C with all other experimental conditions identical (Figure 3, 4). At higher temperature, PDAF-*i*% show enhanced signals at all MI, with maximum enhancements over room temperature values by 34%. Color Doppler is also shown with transducer signals requiring less than half of the power those at room temperature (MI = 0.87 vs. MI = 1.9, Figure 4).

These results demonstrate that the interaction between PFP and PDAF-*i*% is strong enough to maintain stability at body temperature, where the PFP response to 7 MHz US is significantly enhanced. The nature of this stabilization is complex but has been demonstrated in biphasic molecular solutions.^{35, 36} Prior to 1H,1H,2H,2H-perfluorodecanethiol functionalization, the PDA forms a colloidal suspension that is stabilized by the negative zeta potential. This provides the

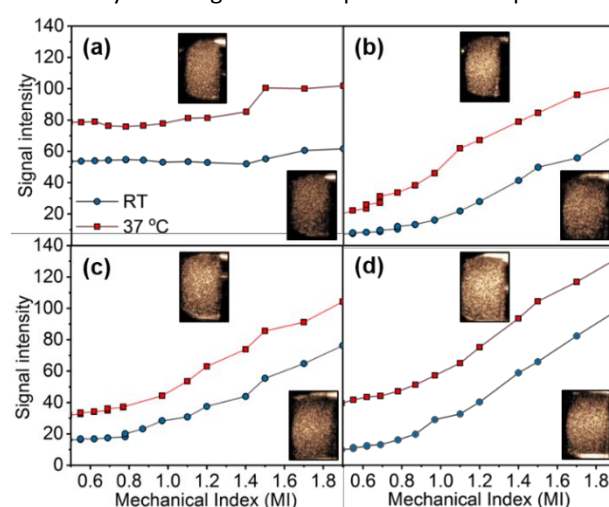


Fig. 3 CPS signal brightness versus Mechanical Index (MI) for (a) PDAF-0.13% NPs, (b) PDAF-1.0% NPs, (c) PDAF-1.7% NPs, and (d) PDAF-2.4%; The MI is a unitless measure of the maximum reduction in pressure induced by the ultrasound wave defined as MI = peak negative pressure / $\sqrt{\text{center frequency of the US beam}}$. Signal brightness is determined by averaging the 8-bit pixel intensities over equivalent ROI for all data. Images in inset are representative CPS data at MI=1.9 for each sample.

polarity necessary for solvation by water and the Coulombic repulsion required to prevent particle aggregation. Upon functionalization with 1H,1H,2H,2H-perfluorodecanethiol, the fluororous areas of the PDAF-*i*% surface become the most stable position for PFP loading. If this loading process induces PDAF-*i*% aggregation, surface-stabilized Pickering emulsions will form (*vide infra*). To demonstrate the importance of the fluorophilic interaction to stabilization, PFP-loading was attempted on samples of PDA-Fe prior to fluorine functionalization. Negligible color Doppler signal was observed at room temperature, confirming that PFP is not retained in this case (Figure 2a and S8c-e).

Given that the robust nature of the fluorophilic stabilization provided by PDAF-*i*% permits strong imaging signals even with elevated temperatures, we were interested in whether we could utilize PFCs with widely differing physical properties to alter the UCA without any redesign of the particle itself. This

would increase their versatility towards different imaging targets emphasizing deep tissue penetration (low frequency) or

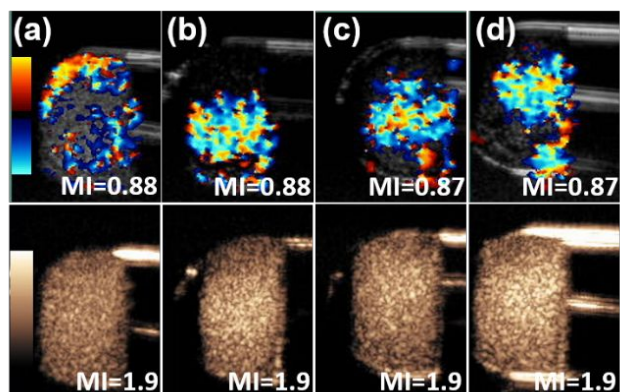


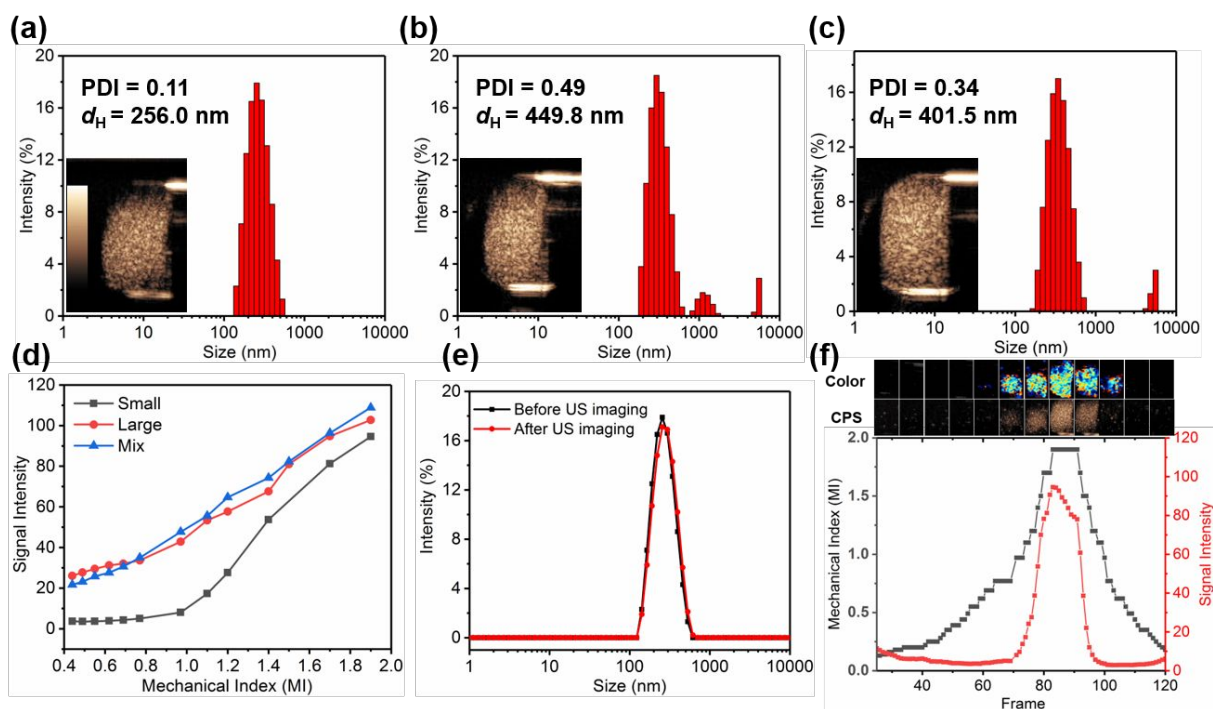
Fig. 4 Color Doppler and CPS imaging of (a) PDAF-0.13% NPs, (b) PDAF-1.0% NPs, (c) PDAF-1.7% NPs, (d) PDAF-2.4% NPs at 37°C.

high resolution (high frequency). For example, Goodwin et al. reported that greater MI was required to induce the vaporization of PFH than PFP, such that high intensity focused ultrasound (HIFU) was required.³⁷ As probes of the versatility of our particles, both PFCs with enhanced (perfluorobutane (PFB), $T_b = -1.7^\circ\text{C}$) and diminished (perfluorohexane (PFH), $T_b = -56^\circ\text{C}$) volatility were imaged using color Doppler and CPS modalities (Figure S10). Despite a range of over 50°C in T_b , the imaging characteristics are remarkably stable (Figure S11), quantitatively in the range of 80-100 at MI = 1.9. These data indicate that a mechanism other than irreversible cavitation may be leading to imaging contrast from these materials, since bubble dynamics will depend strongly on the physical

dissolution from the NP, then it may be possible to design UCAs that image persistently until cleared.

To test long-term continuous imaging capability, PFP-loaded PDAF-*i*% were subjected to continuous MI = 1.5 and 1.9 color Doppler imaging (Figure S12). Commercial UCAs can generally be imaged for less than 30 min before losing signal,³⁸ yet PDAF-2.4% exhibited 6 h of imaging lifetime without dropping to background levels. Given the ability to stabilize during continuous imaging, periodic imaging after long-term storage was also tested. Storage of pre-mixed UCA is generally not possible due to the volatility of PFCs, and so a kit is required to form emulsions for immediate use. To test the stability of PFP-loaded PDAF-*i*%, fully prepared samples in aqueous solution were stored at 4°C and imaged over the course of 50 d (Figure S13). Both color Doppler imaging and CPS remain strong after 50 d indicating long shelf life.

As shown in Figure S5, some amount of aggregation is demonstrated to occur after PFP loading. The ultrasound mechanism and optimization strategy of microparticle and nanoparticle UCAs is fundamentally different and thus determining the signal derived from each subpopulation of PDAF sample is important. In order to distinguish the contribution of ultrasound signal between small nanoparticles and large aggregates, the PFP-loaded PDAF-2.4% particles were separated by low speed centrifugation (2500 rpm, 3 min). Subpopulations from supernatant (named as PDAF-small) and precipitate (PDAF-large) were collected and compared with the original sample (PDAF-mix). DLS data (Figure 5a-c) shows that the hydrodynamic size of PDAF-small ($d = 256\text{ nm}$; PDI = 0.11) is comparable to the non-PFP loaded sample (202 nm, PDI = 0.081; Figure S4d). Both PDAF-large and PDAF-mix (Figure 5b-c) show aggregation with many particles in the 1-5 μm range as



characteristics of the PFC. If imaging can occur without PFC

expected from the original DLS data (Figure S5). In addition to DLS, we performed optical microscopy on particles before,

Fig. 5 DLS size distribution of PFP-loaded (a) PDAF-small, (b) PDAF-large, (c) PDAF-mix with the insets of CPS imaging. (d) Quantitative plot of signal intensity for CPS imaging for PFP-loaded PDAF-small, PDAF-large and PDAF-mix. (e) DLS size distribution of PFP-loaded PDAF-small before and after three cycles of ultrasound imaging. (f) Quantitative analysis of image signal intensity (red) and MI (black) versus frame number for CPS imaging of PFP-loaded PDAF-small particles. The insets are corresponding color Doppler and CPS images according to different frame number.

during, and after exposure to 5 MHz ultrasound excitation (Figure S14). While aggregates were observable in PDAF-large and PDAF-mix, the application of ultrasound did not induce further aggregation in the system. The organization of solid particles to stabilize an interface, known as a Pickering emulsion,³⁹ has been incorporated into ultrasound contrast agents in a number of systems.^{40, 41} To investigate whether the observed aggregates were the source of ultrasound contrast in our samples, individual size sub-populations were analyzed by ultrasound contrast techniques.

After confirming the aggregation state by DLS and optical microscopy, immediate CPS and color Doppler imaging studies were performed on PDAF-small, PDAF-large, and PDAF-mix (Qualitative CPS and color Doppler images were shown in insets of Figure 5a-c, S15c). All samples show strong signal indicative of the presence of an effective contrast agent. By quantitative analysis of CPS data (Figure 5d), both PDAF-large and PDAF-mix demonstrate an enhancement over the signal intensity of PDAF-small, as aggregated particles could contribute strong ultrasound contrast;⁴² however, this difference decreases with increasing MI and is largely gone by MI = 1.9. It could be inferred from this data that PDAF-small is forming aggregation with increasing MI, and thus the similarity at high MI is simply a result of converting PDAF-small into PDAF-large. However, the DLS data shows remarkably stable particle size distribution before and after ultrasound imaging (Figure 5e), and the MI measurement can be cycled repeatedly without a change in the signal response (Figure S15d-e). Perhaps the most interesting finding from the aggregation study is the starkly different curvature to the MI-response between samples. While both PDAF-mix and PDAF-large show a roughly linear signal response to increased MI (Figure 5d, Figure S15a-b), PDAF-small shows negligible response levels until MI = 1.0. At MI > 1.0, the response begins to rapidly increase with MI (Figure 5d). This behavior is seen more clearly when MI and CPS signal are plotted vs individual frame number (Figure 5f, S15d-e). Both CPS and Doppler signals show a “turn on” response consistently around MI = 1.0. Since the transducer frequency is fixed for these studies, this corresponds to either a threshold peak negative pressure (PNP) or a threshold MI (MI = PNP / $\sqrt{\text{center frequency}}$) for this UCA formulation. Overall, these data suggest that both small particles (PDAF-small) and large aggregation (PDAF-large) can contribute ultrasound signal in our system, though their signals have important fundamental differences that will be the subject of future study. For the remainder of the studies discussed, the unseparated PDAF-mixed samples will be used except where explicitly indicated.

Previous results have demonstrated that the imaging characteristics of PDA translate well between aqueous solution, biological buffer, serum, and *ex vivo* tissue.^{10, 22} To ensure the stable and bright contrast of PDAF-*i*% are not limited to solution measurements, *ex vivo* tissue imaging experiments were performed. PFP-loaded PDAF-2.4% was injected into the ventricle of a chicken heart and imaged with color Doppler, B-mode, and CPS ultrasound signals (Figure S16). The most intense area of B-mode imaging shows the position of nanoparticles after injection. However, the signal is difficult to

differentiate from surround tissue, which also exhibits B-mode contrast. Corresponding regions in color Doppler and CPS signal demonstrate the low-background, millimeter-level imaging capabilities of contrast-enhanced ultrasound. The color Doppler speckle pattern reflects the lack of flow in the tissue, indicating the promise of PDAF-*i*% for the *in vivo* studies where differentiation between flow rates is vital for assessing tissue health. For comparison, water injected into the chicken heart tissue shows no signal by either contrast mode (Figure S17).

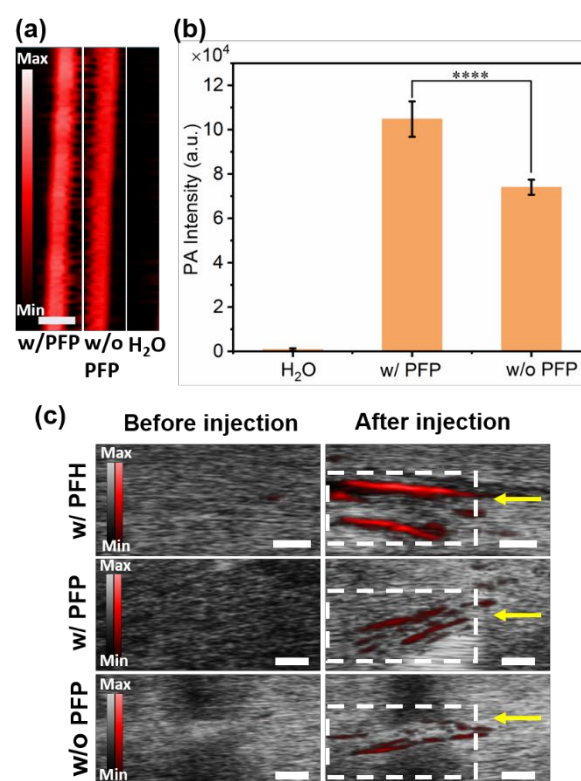


Fig. 6 (a) *In vitro* PA imaging of PDAF-2.4% NPs, with (w/) or without (w/o) PFP loaded at 21 MHz. Scale bar = 2 mm. (b) the corresponding quantitative analysis of PA signal in (a), and the statistical significance was determined with *t* test, *****p* < 0.0001, (c) Combined PA (red color, white-rectangle area) and B-mode (grayscale) *ex vivo* imaging of PDAF-2.4% in chicken breast tissue. The scale bar in panel (c) is 1 mm.

As a complementary tool to conventional ultrasound imaging, photoacoustic (PA) imaging has attracted great research interest because it combines the high contrast and spectral nature of optics with the spatial and temporal resolution of ultrasound.⁴³⁻⁴⁶ The PA signal arises from an optical pulse generating localized pressure waves within a strongly absorbing material such as a plasmonic nanoparticle and organic semiconductors.⁴⁷⁻⁵² Recent work has shown that PDA-based materials show strong PA imaging performance due to their high absorption in the NIR region.^{43, 53} Additionally, traditional UCAs have demonstrated that US/PA dual-modal contrast is a viable technique for biological tissue imaging.⁵⁴ Given the strong absorption of PDAF-*i%* through 1000 nm (Figure S18), it could be expected that PFC-loaded PDAF-*i%* would display a bright PA signal in addition to US. In our study, a Vevo 2100 LAZA PA imaging system (Visualsonics) was used to scan the *in vitro* PA signal of PFP and non-PFP-loaded PDAF-2.4% in aqueous solution (Figure 6). PA imaging and its quantitative analysis are shown in Figure 6a and 6b. Not only is PA imaging possible in PFP-loaded PDAF-2.4%, but it is enhanced by roughly 40% compared with the equivalent non-PFP loaded sample, fitting with previously results on microbubble contrast agents.^{35, 54-56} As shown in ultrasound contrast, particle aggregation in the presence of PFC can be expected to play a role in the PA signal as well. Likely an effect of the enhanced absorption in the aggregates, a stronger signal is indeed observed for PDAF-large (Figure S15f). In addition, the Fe concentration of PDAF-*i%* was expected to play a role in PA imaging contrast due to charge transfer absorption involving the chelation to the PDA catecholate (Figure 7a,b).¹⁸ Interestingly, we observe a drastic PA enhancement when comparing PDAF-0.13% and all other samples. Since this trend correlates with the particle size variation as well as the Fe³⁺ content, the contribution of each factor to the PA signal cannot be deconvoluted. It is, however, consistent with a previous report⁵⁷ and with the much lower extinction coefficient of PDAF-0.13% compared to that of other PDAF-*i%* samples (Figure 7c).

Ex vivo PA imaging of PDA particles in chicken breast tissue was also performed (Figure 6c, S19). PFP-, PFP- and no PFC-loaded PDAF-2.4% were injected 1 cm into the chicken breast tissue and subsequently imaged at the injection site at 40 MHz.

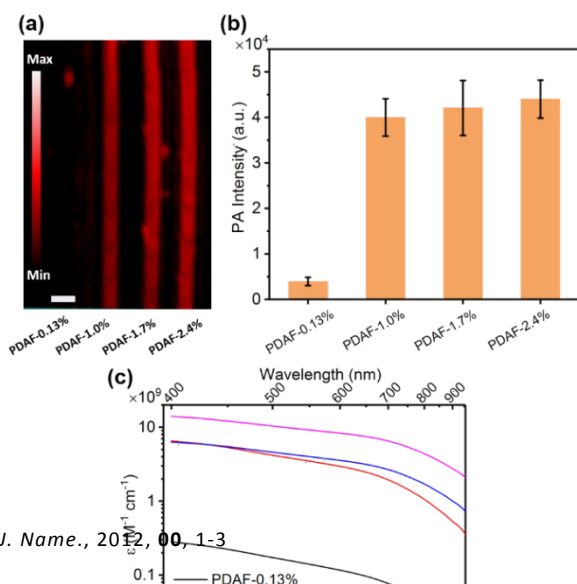
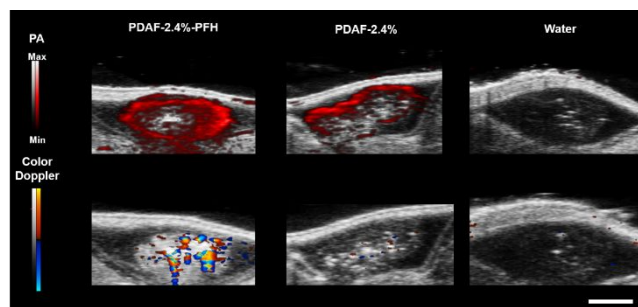


Fig. 7 (a) *In vitro* PA imaging of PDAF-*i%* NPs under 0.5 mg mL⁻¹ at 21 MHz, (b) the corresponding quantitative analysis of PA signal in (a), (c) molar volume extinction coefficient of PDAF-*i%*. The scale bar in panel (a) is 2 mm.



The PA signal appears in the striations of the muscle fiber in the chicken breast tissue after the injection of nanoparticles,

indicated by the red line in the Figure 6c. It should be noted that there is observable signal increase with PFC-loaded PDA samples compared with no PFC-loaded PDA samples, in agreement with the *in vitro* PA imaging results.

PDA is chemically similar to natural melanin and has been shown to be biocompatible in various synthetic forms. Figure S20 reveals that cell viability of all PDAF-*i%* is greater than 80% at all concentrations for HCT116 cells, indicating good biocompatibility for PDAF-*i%*.

The PFP-loaded PDAF-*i%* exhibits stable *in vivo* PA and color

Fig. 8 *In vivo* PA and color Doppler imaging with PFP-loaded PDAF-2.4% (2 mg mL⁻¹), PDAF-2.4% without PFP, and water control. Scale bar represents 2 mm.

Doppler signal under constant laser exposure. The subcutaneously injected PFP-loaded PDAF-2.4% had 1.5 and 146.2-fold stronger PA intensity, with significantly higher color Doppler signal, than the negative controls PDAF-2.4% and Millipore water mixed with Matrigel in a 1:1 ratio (Figure 8). Furthermore, the PA and color Doppler signal of the PFP-loaded PDAF-2.4% remained stable (RSD < 2.3%, Figure S21) during constant 700 nm laser excitation for 30 minutes with a detection limit of 0.12 mg/mL in the PA mode and ~2.0 mg/mL in the color Doppler mode (Figure S22). These results demonstrated the long-term *in vivo* utility of the PFP loaded PDAF-*i%* particles.

Overall, PDAF-*i%* demonstrate promising characteristics as UCAs: (1) They display strong contrast by both color Doppler and CPS imaging techniques; (2) the fluorophilic mode of PFC stabilization presents a way to image that is largely orthogonal to other tunable characteristics. Thus, synthetic handles such as size, metal content, constituent monomer can be repurposed to control tissue penetration, deliver alternate modes of contrast, or trigger therapeutic responses; (3) the stability of the PFC/particle interaction allows for long-term continuous imaging ability, which can be used as the contrast agents for tissue imaging. This long-timescale ability could allow for long-term tracking of flow patterns and analysis of flow on tissue perfusion timescales.

Conclusions

In vitro US imaging at 20°C and 37°C both show remarkable contrast pulse sequences (CPS) and color Doppler signal at MI = 1.9; and significant color Doppler signal could be found at MI =

0.87 at 37°C. It should be noted that our PDAF-*i*% NPs could be imaged at MI = 1.9 for at least 6 h and were effective after storage at 4°C for almost two months, a behavior markedly different from other type of microbubble-based agents as well as our previous PDA-F NPs.¹⁰ Often in nanoparticle-based ultrasound UCAs, it is difficult to characterize the extent to which aggregation plays a role in the properties. Optimization of our initial size distribution and careful separation by low speed centrifugation and immediate characterization have allowed us to address key differences due to nanoparticle aggregations. Importantly, our results indicate that both isolated particles and aggregations contribute to the overall signal we observe, but the differences are not simply in signal magnitude. Specifically, the threshold MI response for PDAF-small warrants further study and may hold cues as to the methods to further control and optimize this signal response. Future work will continue to push the limits of these materials to longer imaging time and more optimized ultrasound response via tuning the particle design. Given the wide known parameter space for modification of polymer nanoparticles, further capabilities should be available, such as triggered positive contrast and multi-color contrast. This synthetic control of functionality offers the exciting possibility of specializing UCAs analogous to more established contrast agents like those of MRI, which have benefitted strongly from fundamental exploratory research into their structure-property relationships.

Conflicts of interest

There are no conflicts to declare.

Acknowledgements

The authors acknowledge support from the Air Force Office of Scientific Research MURI (FA9550-18-1-0142). We also acknowledge the characterization facilities provided by the National Center for Microscopy and Imaging Research (NCMIR), STEM-EDS and XPS supported by the BioCryo facility, and the Keck-II facilities of Northwestern University's NUANCE Center. This work was performed in part at the San Diego Nanotechnology Infrastructure (SDNI) of UCSD, a member of the National Nanotechnology Coordinated Infrastructure, which is supported by the National Science Foundation (Grant ECCS-1542148). Prof. Jesse V. Jokerst acknowledges support from NIH HL 137187, HL 117048, and OD OD021821.

References

- W. Cai and X. Chen, *Small*, 2007, **3**, 1840-1854.
- E. Terreno, D. D. Castelli, A. Viale and S. Aime, *Chem. Rev.*, 2010, **110**, 3019-3042.
- X. Qian, X. Han and Y. Chen, *Biomaterials*, 2017, **142**, 13-30.
- K. W. Ferrara, M. A. Borden and H. Zhang, *Acc. Chem. Res.*, 2009, **42**, 881-892.
- M. A. Nakatsuka, R. F. Mattrey, S. C. Esener, J. N. Cha and A. P. Goodwin, *Adv. Mater.*, 2012, **24**, 6010-6016.
- F. Yang, S. Hu, Y. Zhang, X. Cai, Y. Huang, F. Wang, S. Wen, G. Teng and N. Gu, *Adv. Mater.*, 2012, **24**, 5205-5211.
- S. R. Sirsi and M. A. Borden, *Bubble Sci. Eng. Technol.*, 2009, **1**, 3-17.
- E. G. Schutt, D. H. Klein, R. M. Mattrey and J. G. Riess, *Angew. Chem., Int. Ed.*, 2003, **42**, 3218-3235.
- Y. Zhou, Z. Wang, Y. Chen, H. Shen, Z. Luo, A. Li, Q. Wang, H. Ran, P. Li, W. Song, Z. Yang, H. Chen, Z. Wang, G. Lu and Y. Zheng, *Adv. Mater.*, 2013, **25**, 4123-4130.
- Y. Xie, J. Wang, Z. Wang, K. A. Krug and J. D. Rinehart, *Nanoscale*, 2018, **10**, 12813-12819.
- C.-F. Su, H. Merlitz, H. Rabbel and J.-U. Sommer, *J. Phys. Chem. Lett.*, 2017, **8**, 4069-4076.
- Q.-Y. Bao, A.-Y. Liu, Y. Ma, H. Chen, J. Hong, W.-B. Shen, C. Zhang and Y. Ding, *Colloids Surf. B*, 2016, **146**, 475-481.
- S. U. Pickering, *J. Chem. Soc., Trans.*, 1907, **91**, 2001-2021.
- D. S. Li, S. Schneewind, M. Bruce, Z. Khaing, M. O'Donnell and L. Pozzo, *Nano Lett.*, 2019, **19**, 173-181.
- D. S. Li, Y.-T. Lee, Y. Xi, I. Pelivanov, M. O'Donnell and L. D. Pozzo, *Soft Matter*, 2018, **14**, 5283-5293.
- J. E. Lemaster, F. Chen, T. Kim, A. Hariri and J. V. Jokerst, *ACS Appl. Nano Mater.*, 2018, **1**, 1321-1331.
- J. Wang, C.-Y. Lin, C. Moore, A. Jhunjunwala and J. V. Jokerst, *Langmuir*, 2018, **34**, 359-365.
- Y. Li, Y. Xie, Z. Wang, N. Zang, F. Carniato, Y. Huang, C. M. Andolina, L. R. Parent, T. B. Ditri, E. D. Walter, M. Botta, J. D. Rinehart and N. C. Gianneschi, *ACS Nano*, 2016, **10**, 10186-10194.
- Z. Wang, Y. Xie, Y. Li, Y. Huang, L. R. Parent, T. Ditri, N. Zang, J. D. Rinehart and N. C. Gianneschi, *Chem. Mater.*, 2017, **29**, 8195-8201.
- Z. Wang, F. Carniato, Y. Xie, Y. Huang, Y. Li, S. He, N. Zang, J. D. Rinehart, M. Botta and N. C. Gianneschi, *Small*, 2017, **13**, 1701830.
- D. Hu, C. Liu, L. Song, H. Cui, G. Gao, P. Liu, Z. Sheng and L. Cai, *Nanoscale*, 2016, **8**, 17150-17158.
- J. Sun, W. Xu, L. Li, B. Fan, X. Peng, B. Qu, L. Wang, T. Li, S. Li and R. Zhang, *Nanoscale*, 2018, **10**, 10584-10595.
- J. Cui, Y. Yan, G. K. Such, K. Liang, C. J. Ochs, A. Postma and F. Caruso, *Biomacromolecules*, 2012, **13**, 2225-2228.
- Y. Li, C. Jiang, D. Zhang, Y. Wang, X. Ren, K. Ai, X. Chen and L. Lu, *Acta Biomater.*, 2017, **47**, 124-134.
- Y. Liu, K. Ai, J. Liu, M. Deng, Y. He and L. Lu, *Adv. Mater.*, 2012, **25**, 1353-1359.
- R. Ge, M. Lin, X. Li, S. Liu, W. Wang, S. Li, X. Zhang, Y. Liu, L. Liu, F. Shi, H. Sun, H. Zhang and B. Yang, *ACS Appl. Mater. Interfaces*, 2017, **9**, 19706-19716.
- Q. Yue, M. Wang, Z. Sun, C. Wang, C. Wang, Y. Deng and D. Zhao, *J. Mater. Chem. B*, 2013, **1**, 6085-6093.
- G. Picheth, S. Houvenagel, C. Dejean, O. Couture, R. Alves de Freitas, L. Moine and N. Tsapis, *Acta Biomater.*, 2017, **64**, 313-322.
- M. D. Abràmoff, P. J. Magalhães and S. J. Ram, *Biophotonics Intern.*, 2004, **11**, 36-42.
- G. M. Veith and N. J. Dudney, *J. Electrochem. Soc.*, 2011, **158**, A658-A663.
- A. Liberman, J. Wang, N. Lu, R. D. Viveros, C. A. Allen, R. F. Mattrey, S. L. Blair, W. C. Trogler, M. J. Kim and A. C. Kummel, *Adv. Funct. Mater.*, 2015, **25**, 4049-4057.
- J. F. Synnevag, A. Austeng and S. Holm, *IEEE Trans. Ultrason., Ferroelectr., Freq. Control*, 2007, **54**, 1606-1613.

33. A. Liberman, Z. Wu, C. V. Barback, R. Viveros, S. L. Blair, L. G. Ellies, D. R. Vera, R. F. Mattrey, A. C. Kummel and W. C. Trogler, *ACS Nano*, 2013, **7**, 6367-6377.
34. H. Ke, J. Wang, Z. Dai, Y. Jin, E. Qu, Z. Xing, C. Guo, X. Yue and J. Liu, *Angew. Chem., Int. Ed.*, 2011, **50**, 3017-3021.
35. D. Y. Santiesteban, D. S. Dumani, D. Profili and S. Y. Emelianov, *Nano Lett.*, 2017, **17**, 5984-5989.
36. D. A. Fernandes, D. D. Fernandes, Y. Li, Y. Wang, Z. Zhang, D. Rousseau, C. C. Gradinaru and M. C. Kolios, *Langmuir*, 2016, **32**, 10870-10880.
37. N. T. Blum, A. Yildirim, R. Chattaraj and A. P. Goodwin, *Theranostics*, 2017, **7**, 694-702.
38. J. Wang, C. V. Barback, C. N. Ta, J. Weeks, N. Gude, R. F. Mattrey, S. L. Blair, W. C. Trogler, H. Lee and A. C. Kummel, *IEEE Trans. Med. Imaging*, 2017, **37**, 222-229.
39. Y. Chevalier and M.-A. Bolzinger, *Colloids Surf., A*, 2013, **439**, 23-34.
40. Ý. Mørch, R. Hansen, S. Berg, A. K. O. Åslund, W. R. Glomm, S. Eggen, R. Schmid, H. Johnsen, S. Kubowicz, S. Snipstad, E. Sulheim, S. Hak, G. Singh, B. H. McDonagh, H. Blom, C. de Lange Davies and P. M. Stenstad, *Contrast Media Mol. Imaging*, 2015, **10**, 356-366.
41. J. Wu and G.-H. Ma, *Small*, 2016, **12**, 4633-4648.
42. F. Calliada, R. Campani, O. Bottinelli, A. Bozzini and M. G. Sommaruga, *Eur. J. Radiol.*, 1998, **27**, S157-S160.
43. Z. Dong, L. Feng, Y. Hao, M. Chen, M. Gao, Y. Chao, H. Zhao, W. Zhu, J. Liu, C. Liang, Q. Zhang and Z. Liu, *J. Am. Chem. Soc.*, 2018, **140**, 2165-2178.
44. J. Weber, P. C. Beard and S. E. Bohndiek, *Nat. Meth.*, 2016, **13**, 639.
45. A. De La Zerda, C. Zavaleta, S. Keren, S. Vaithilingam, S. Bodapati, Z. Liu, J. Levi, B. R. Smith, T.-J. Ma, O. Oralkan, Z. Cheng, X. Chen, H. Dai, B. T. Khuri-Yakub and S. S. Gambhir, *Nat. Nanotechnol.*, 2008, **3**, 557.
46. M. Xu and L. V. Wang, *Rev. Sci. Instrum.*, 2006, **77**, 041101.
47. C. Tian, W. Qian, X. Shao, Z. Xie, X. Cheng, S. Liu, Q. Cheng, B. Liu and X. Wang, *Adv. Sci.*, 2016, **3**, 1600237.
48. S. Mallidi, T. Larson, J. Tam, P. P. Joshi, A. Karpouk, K. Sokolov and S. Emelianov, *Nano Lett.*, 2009, **9**, 2825-2831.
49. W. Tang, Z. Yang, S. Wang, Z. Wang, J. Song, G. Yu, W. Fan, Y. Dai, J. Wang, L. Shan, G. Niu, Q. Fan and X. Chen, *ACS Nano*, 2018, **12**, 2610-2622.
50. Z. Yang, R. Tian, J. Wu, Q. Fan, B. C. Yung, G. Niu, O. Jacobson, Z. Wang, G. Liu, G. Yu, W. Huang, J. Song and X. Chen, *ACS Nano*, 2017, **11**, 4247-4255.
51. Z. Yang, W. Fan, W. Tang, Z. Shen, Y. Dai, J. Song, Z. Wang, Y. Liu, L. Lin, L. Shan, Y. Liu, O. Jacobson, P. Rong, W. Wang and X. Chen, *Angew. Chem., Int. Ed.*, 2018, **130**, 14297-14301.
52. Z. Yang, Y. Dai, C. Yin, Q. Fan, W. Zhang, J. Song, G. Yu, W. Tang, W. Fan, B. C. Yung, J. Li, X. Li, X. Li, Y. Tang, W. Huang, J. Song and X. Chen, *Adv. Mater.*, 2018, **30**, 1707509.
53. H. Zhu, D. Qin, Y. Wu, B. Jing, J. Liu, D. Hazlewood, H. Zhang, Y. Feng, X. Yang, M. Wan and D. Wu, *ACS Appl. Mater. Interfaces*, 2018, **10**, 29251-29259.
54. R. X. Xu, *Contrast Media Mol. Imaging*, 2011, **6**, 401-411.
55. C. Kim, R. Qin, J. S. Xu, L. V. Wang and R. X. Xu, *J. Biomed. Opt.*, 2010, **15**, 010510.
56. K. Wilson, K. Homan and S. Emelianov, *Nat. Commun.*, 2012, **3**, 618.
57. J. E. Lemaster, Z. Wang, A. Hariri, F. Chen, Z. Hu, Y. Huang, C. V. Barback, R. Cochran, N. C. Gianneschi and J. V. Jokerst, *Chem. Mater.*, 2019, **31**, 251-259.